IIETA International Information and Engineering Technology Association
Advancing the World of Information and Engineering

International Journal of Heat and Technology
Vol. 36, No. 2, June, 2018, pp. 619-631
Journal homepage: http://iieta.org/Journals/IJHT

Natural convection in polyethylene glycol based molybdenum disulfide nanofluid with thermal radiation, chemical reaction and ramped wall temperature

Farhad Ali[1,2*], Muhammad Arif[3], Ilyas Khan[4], Nadeem A. Sheikh[3], Muhammad Saqib[3,5]

[1] Computational Analysis Research Group, Ton Duc Thang University, Ho Chi Minh City 700000, Vietnam
[2] Faculty of Mathematics and Statistics, Ton Duc Thang University, Ho Chi Minh City 700000, Vietnam
[3] Department of Mathematics, City University of Science and Information Technology, Peshawar, Khyber Pakhtunkhwa 25000, Pakistan
[4] Basic Engineering Sciences Department, College of Engineering Majmaah University, Majmaah 11952, Saudi Arabia
[5] Department of Mathematical sciences, Faculty of Science, Universiti Teknologi Malaysia, Skudai 81310 UTM Johar Bahru, Malysia

Corresponding Author Email: farhad.ali@tdt.edu.vn

https://doi.org/10.18280/ijht.360227

Received: 23 November 2017
Accepted: 27 April 2018

Keywords:
PEG, molybdenum disulfide (MoS_2) *, Casson nanofluid, ramped wall temperature*

ABSTRACT

The aim of this study is to investigate the unsteady magnetohydrodynamic (MHD) flow of Casson nanofluid over an infinite oscillating vertical plate with ramped wall temperature. The effects of porosity, thermal radiation and first order chemical reaction have been considered. Polyethylene glycol (PEG) is chosen as base fluid which contained molybdenum disulfide (MoS_2) nanoparticles. The Laplace transform technique is applied to the momentum, energy and concentration equations to obtain the closed form solutions. The obtained solutions are for both cases ramped and isothermal boundary conditions and compared graphically. From graphical analysis, it is observed that for isothermal plate, the magnitude of velocity, temperature and concentration profiles are greater than ramped wall temperature. Skin-friction, Nusselt number and Sherwood number are evaluated and presented in tabular forms. The effects of various embedded parameters on velocity, temperature and concentration profiles are discussed graphically.

1. INTRODUCTION

The effect of heat and mass transfer phenomena occurs due to the differences in temperature and concentration. In modern technology heat and mass transfer phenomena plays a key role, especially in engineering, due to this reason most of the researchers are attracted to further investigate on this topic.

Moreover, heat and mass transfer have a wide range of industrial and practical life applications, like freeze-drying phenomena of food [1]. Blums [2], Incropera and De Witt [3] discussed in details on heat and mass transfer with several thermal and concentration applications. The phenomenon of heat and mass transfer, is very important because of many physical uses in science and modern technology as discussed in the book of Nield and Bejan [4].

The thermal conductivity of a fluid is also important in modern technology. In the literature, different methods have been produced to increase the concentration and temperature transfer performance of the fluids. To improve the thermal conductivity of the conventional base fluids like polyethylene glycol (PEG), ethylene glycol (EG) and oil mixture by adding some microparticles or large-sized particles in the fluid. But, the addition of these particles induces additional flow resistance and erosion. The type of fluid in which nanoparticles are added is called a nanofluid. The addition of nanoparticles results in an increase in the thermal performance of the base fluid. Choi [5] for the first time discussed nanofluid in Argonne National Laboratory. He explained that suspension of nanoparticles in the fluid can be considered as heat transfer fluids. Furthermore, he also noted that the heat transfer performance rate of nanofluid is greater as compared to pure liquids. He found that nanofluids have maximum heat transfer properties compared to fluids containing micro-sized particles. In another paper, Choi et al. [6] discussed the process when some nanoparticles are added to the base fluid which increased the thermal performance of the fluid approximately, two times. Many researchers like Li and Eastman [7], Masuda et al. [8], and Xuan and Roetzel [9] examined that the addition of nano-sized particles increase heat transfer rate more than 20%. The thermal performance rate of these fluids depends upon the factors like molecule volume species, nanoparticles size, nanoparticles shape and other physical properties of the base fluid like temperature and concentration of the base fluid materials. Nanoparticles which are used in nanofluids can be prepared from different materials by using chemical and physical synthesis processes. Wakif et al. [10] numerically analyzed the onset of longitudinal convective flow of nanofluids with an external magnetic field rolls in a porous medium. Ali et al. [11] investigated the effect of MHD nanofluid with engine oil base fluid and taking Mos_2 nanoparticles in a rotating disk with hall effect.

There are some non-Newtonian fluids in nature whose behavior is that by decreasing viscosity there is an increase in velocity gradient e.g. polymer solutions, blood, elastic solid etc. that is, with a small shear stress, no flow is occurring. Casson fluid is one of those fluids which has distinct features

and is very famous in recent research. Casson in 1959 [12] modeled and introduced Casson fluid for the prediction of pigment oil suspensions of the flow behavior. Casson fluid is one of the pseudoplastic that means shear thinning fluids. At minimum shear rates, the fluid which is shear thinning is more viscous as compare to a Newtonian fluid. Dash et al. [13] discussed non-Newtonian Casson fluid in a pipe filled with homogeneous porous medium. Akbar [14], Noreen and Butt [15] and Nadeem et al. [16-17] investigated Casson fluid flow in a plumb duct/asymmetric channel. Saqib et al. [18] discussed heat and mass transfer phenomena for the flow of non-Newtonian Casson fluid over an infinite oscillating vertical plate, taking slip effect on the boundary and first-order chemical reaction. The influence of induced magnetic field on the flow of Casson fluid is investigated by Raju et al. [19]. Recently researchers are interested in studying some non-Newtonian fluids like Casson fluids etc. These fluids have an important role in modern technology. Qing et al. [20] worked out on entropy generation taking the effect of MHD Casson nanofluid and considered the surface of the flow over a porous stretching/shrinking surface. Mustafa and Khan [21], studied a model for the flow of Casson nanofluid past over a nonlinearly stretching sheet and taking the effect magnetic field. Casson nanofluid. Haq et al. [22] published their work on Convective heat transfer and MHD effects on Casson nanofluid flow over a shrinking sheet. Nadeem et al. [23] investigated Casson nanofluid with convective boundary conditions. Hussain et al. [24] also studied Casson nanofluid with convective conditions and viscous dissipation.

The study of MHD flow has many practical applications especially in engineering problems like nuclear reactors, study related to plasma, MHD generators and geothermal energy aerodynamics [25]. To study the effects of heat and mass transfer in the electrically conducting fluid and the analytical solutions for these problems are unique to a great extent. Heat and mass transfer MHD flow can be solved by different simplifying assumptions [26]. The person who discovered the field of MHD was Alfven and got the Nobel Prize for his new work in 1970. The MHD flow of heat and mass transfer has many industrial applications like preparation of solid plastic film and artificial materials plastic fiber etc. Another important field of application is propulsion of electromagnetism. This system contains a source of power (like a nuclear reactor), plasma and instrument that passes plasma by MHD forces.

In the recent literature, the fluid flow through a porous media has become an attractive topic because of extraction of the crude oil from the openings of the storage of rocks, and more other applications. Furthermore, the theoretical results of heat and mass transfer problems through porous media having many physical applications, such as underground water impurity, geothermal energy reconstruction, thermal storage of energy, flow through distillation media and crude oil extraction. Recently, Kataria and Patel [27] has considered the effect radiation and chemical reaction on MHD Casson fluid flow past over an oscillating vertical plate embedded in porous medium. Ali et al. [28], considered the effect of MHD flow of water-based Brinkman type nanofluid over a vertical plate embedded in a porous medium with variable surface velocity, temperature and concentration.

Mass transfer effect is very important in polymer and chemical processing equipment [29]. In chemical engineering, different processes have done under the chemical reaction which takes place between the fluid under discussion and an external concentration. There are different chemical processes, some of them are known as homogeneous or heterogeneous processes. This chemical process depends on the reaction occurs at an interface. Cussler [30] investigated the effect of homogenous reaction uniformly through a given phase. In many physical situations, it is noticed that rate of chemical reaction depends on the mass and chemical behavior of the species itself. The chemical reactions in which the reaction rate is directly proportional to concentration are called first order chemical reaction [31]. Rajesh [32] performed an experiment to investigate the effect of thermal radiation and first order chemical reaction effects and th fluid is flowing past over a vertical plate with ramped wall temperature condition.

All the above studies take the continuous and well-defined conditions for velocity and temperature at the wall. But, in many physical problems and practical situations, there are some non-uniform wall conditions. To investigate such problems, it is necessary to introduce the condition of ramped wall temperature. In many physical situations, for example, the process of different materials, nuclear heat transfer control, heat transfer in building, heat transfer in the turbine, and some electric circuits etc. has useful applications of ramped condition at the wall temperature. Due to this fact researchers are focused some problems related to free convection from an infinite vertical plate and the condition at the wall is taken as ramped wall temperature. Kelleher [33] and Kao [34] earlier investigated the flow of free convection with ramped wall temperature. Having such kind of motivations, Chandran et al. [35] presented their work on the unsteady flow of natural convection with ramped condition of a temperature at the wall. Seth et al. [36] discussed MHD flow with radiative heat transfer and considered the effect of porous medium and ramped wall temperature condition at the plate. The effect of radiation on the fluid flow, over an infinite vertical plate with ramped wall temperature and consider mass diffusion constant was discussed by Narahari and Beg [37]. The exact solutions for the flow of nanofluids with ramped condition of temperature were investigated by Khalid et al. [38]. Khan et al. [39] explained MHD free convection flow and consider the effect of porous media and ramped wall temperature. Nandkeolyar et al. [40] studied the flow of unsteady hydromagnetic radiative nanofluid flow over a flat plate and consider the motion of the plate with ramped wall temperature.

In the literature, no work is reported to obtain the closed form solutions for the MHD Casson nanofluid flow over an infinite vertical plate with the effects of porous media and ramped wall temperature condition. Therefore, the objective of the study is to fill the gap and to find the exact solutions of MHD Casson nanofluid past an infinite vertical plate embedded in a porous medium. The effects of thermal radiation and chemical reaction of the first order are also considered in this problem. Furthermore, we have considered molybdenum disulfide (MoS_2) nanoparticles suspended in the base fluid polyethylene glycol (PEG). The most attractive work of the given study is to compare the ramped wall and isothermal boundary conditions graphically for velocity, temperature and concentration profiles. The parametric study of constants like, magnetic parameter M, thermal Grashof number Gr, mass Grashof number Gm, Schmidt number Sc, radiation parameter, chemical reaction parameter and porous medium K are preformed graphically. The effects of various embedded parameters on skin-friction, Nusselt number and Sherwood number have been shown in tabular form. The exact solutions for the above problem have been obtained by using Laplace transform technique.

2. MATHEMATICAL FORMULATION AND SOLUTION OF THE PROBLEM

The free convection flow of radiative heat and mass transfer of Casson fluid with nanoparticles, is considered. MoS_2 nanoparticles are added to base fluid PEG. It is assumed that the fluid is electrically conducting and lies over an infinite oscillating vertical plate. The fluid flow will be along the x direction in a porous medium parallel to the plate. The fluid will occupy the space at positive y axis where y is perpendicular to the plate. A uniform magnetic field B of strength B_0 is applied in a perpendicular direction to the flow of fluid as shown in figure 1.

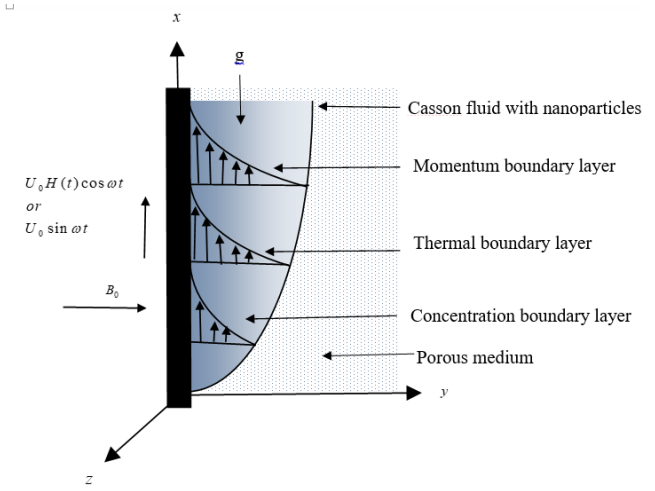

Figure 1. Geometry of the problem

The induced magnetic field will be ignored because of very small Reynolds number. And assumed the effect of chemical reaction of order first, MHD, porosity and ramped wall temperature condition.

Initially, at time *t=0*, the fluid and plate are stationary with ambient temperature and concentration T_∞ and C_∞ respectively. At time $t=0^+$, the plate starts oscillatory motion and the velocity component in x direction is given by

$$u = U_o H(t)\cos\omega t \text{ or } u = U_0 \sin\omega t;\ t > 0 \tag{1}$$

According to the assumptions, the plate will start oscillatory motion in the plane at $(y=0)$. Where U_0 represents constant velocity, $H(t)$ shows Heaviside unit step function, i is the unit vector along x -axis which shows the vertical flow direction and ω is used to represent the symbol of the frequency of oscillations of the plate. At the time, $t=0^+$, the temperature of the plate, as well as concentration, is higher or lower to $T_\infty + (T_w - T_\infty)t/t_0$ and $C_\infty + (C_w - C_\infty)t/t_0$ when $t < t_0$, respectively. When $t \geq t_0$, then there is no change in temperature and concentration, it maintains constant temperature T_w and concentration C_w.

Under assumptions considered in the problem, the dimensional governing equations of the problem are given below [41]:

$$\rho_{nf}\frac{\partial u(y,t)}{\partial t} = \mu_{nf}\left(1+\frac{1}{\beta}\right)\frac{\partial^2 u(y,t)}{\partial y^2}$$
$$-\sigma_{nf}B_0^{\,2}u(y,t) - \left(1+\frac{1}{\beta}\right)\frac{\mu_{nf}\phi}{k_1}u(y,t) \tag{2}$$
$$+g(\rho\beta_T)_{nf}(T-T_\infty) + g(\rho\beta_C)_{nf}(C-C_\infty),$$

$$(\rho C_p)_{nf}\frac{\partial T(y,t)}{\partial t} = k_{nf}\frac{\partial^2 T(y,t)}{\partial y^2} - \frac{\partial q_r}{\partial y}, \tag{3}$$

$$\frac{\partial C(y,t)}{\partial t} = D_{nf}\frac{\partial^2 C(y,t)}{\partial y^2} - K(C-C_\infty). \tag{4}$$

Subject to the following initial and boundary conditions:

$$u(y,0)=0, \qquad T(y,0)=T_\infty, \qquad C(y,0)=C_\infty,$$
$$u(0,t)=U_0H(t)\cos(\omega t) \quad or \quad U_0\sin(\omega t),$$
$$T(0,t)=\begin{cases} T_\infty + (T_w+T_\infty)\dfrac{t}{t_0} & if\ 0<t<t_0 \\ T_w & if\ t\geq t_0 \end{cases}, \tag{5}$$
$$C(0,t)=\begin{cases} C_\infty + (C_w-C_\infty)\dfrac{t}{t_0} & if\ 0<t<t_0, \\ C_w & if\ t\geq t_0, \end{cases}$$
$$u(\infty,t)=0, \qquad T(\infty,t)=T_\infty, \qquad C(\infty,t)=C_\infty.$$

Here u represents the velocity of the fluid along x direction, T and C represents temperature and concentration of the fluid, ρ_{nf}, μ_{nf} and σ_{nf} represents the density, dynamic viscosity and electrical conductivity of nanofluid respectively, β is the Casson fluid parameter, $\phi(0<\phi<1)k_1>0$ where ϕ is the porous medium and k_1 is the permeability of porous medium, $(\beta_T)_{nf}$ and $(\beta_C)_{nf}$ is the thermal expansion coefficient and concentration coefficient of nanofluids respectively, $(C_p)_{nf}$ is the specific heat of nanofluids, k_{nf} is the thermal conductivity of nanofluids, q_r is the radiative heat flux, D_{nf} is the mass diffusivity and K is the chemical reaction parameter which is known as first order chemical reaction.

Where the following expressions are restricted to spherical shape nanoparticles and the effective thermal conductivity of nanofluid given by Kakac and Pramuanjaroenkij [42] and Oztop and Abu-Nada [43] is given by

$$\rho_{nf} = (1-\phi)\rho_f + \phi\rho_s, \quad \mu_{nf} = \frac{\mu_f}{(1-\phi)^{2.5}},$$
$$\sigma_{nf} = \sigma_f\left[1+\frac{3(\sigma-1)\phi}{(\sigma+2)-(\sigma-1)\phi}\right], \sigma = \frac{\sigma_s}{\sigma_f},$$
$$(\rho\beta_T)_{nf} = (1-\phi)(\rho\beta_T)_f + \phi(\rho\beta_T)_s, a_0 = \left[1+\frac{3(\sigma-1)\phi}{(\sigma+2)-(\sigma-1)\phi}\right]$$
$$(\rho\beta_C)_{nf} = (1-\phi)(\rho\beta_C)_f + \phi(\rho\beta_C)_s,$$

$$k_{nf} = k_f\left[1-3\frac{\phi(k_f-k_s)}{2k_f+k_s+\phi(k_f-k_s)}\right],$$

$$\lambda_{nf} = \left[1-3\frac{\phi(k_f-k_s)}{2k_f+k_s+\phi(k_f-k_s)}\right], \quad \lambda_{nf} = \frac{k_{nf}}{k_f},$$

$$\left(\rho C_p\right)_{nf} = (1-\phi)(\rho C_p)_f + \phi(\rho C_p)_s,\ D_{nf} = (1-\phi)D_f,$$

where ϕ the volume fraction of nanoparticles, ρ_f is the base fluid density, ρ_s is the density of the solid particle, C_p is the specific heat at constant pressure.

The radiative heat flux q_r is given below:

$$q_r = \frac{-4\sigma_1}{3k_3}\frac{\partial T^4}{\partial y}, \tag{6}$$

where Sefan-Boltzmann constant is σ_1 and k_3 is the mean absorption coefficient. It is assumed that the temperature difference during the flow is sufficiently very small and the term T^4 can be linearized by Taylor series expansion. Neglecting high order terms in $(T-T_\infty)$, we get:

$$T^4 = 4TT_\infty^{\ 3} - 3T_\infty^{\ 4}. \tag{7}$$

Substituting equation (7) into equation (6) and differentiating with respect to y, we get

$$\frac{\partial q_r}{\partial y} = -\frac{16\sigma_1}{3k_3}T_\infty^{\ 3}\frac{\partial^2 T}{\partial y^2}. \tag{8}$$

Table 1. Thermo-physical properties of PEG and MoS_2

Model	ρ (kgm^{-3})	C_p $(Kg^{-1}K^{-1})$	k $(Wm^{-1}K^{-1})$	$\beta\times10^{-5}$ (K^{-1})	σ (S/m)	υ $\left(m^2.s^{-1}\right)$	Pr
PEG	1128	1500	0.22	60	5.5×10^{-6}	2.387	18.358
MoS2	5.06×10^{3}	397.21	904.4	2.8424	2.09×10^{-4}	-	-

For dimensional analysis introducing the following dimensionless variables

$$u^* = \frac{u}{U_0}, \qquad y^* = \frac{y}{\sqrt{\upsilon t_0}}, \qquad t^* = \frac{t}{t_0},$$

$$\theta = \frac{T-T_\infty}{T_w-T_\infty}, t_0 = \left(\frac{\sqrt{\upsilon}}{g\beta(T_w-T_\infty)}\right)^{\frac{2}{3}};$$

Using dimensionless variables into eqs. (2)- (5), we get the following system of equations:

$$\frac{\partial u}{\partial t} = a_1\frac{\partial^2 u}{\partial y^2} - Hu + Gra_2\theta + Gma_3\Phi, \tag{9}$$

$$P_0\frac{\partial\theta}{\partial t} = \frac{\partial^2\theta}{\partial y^2}, \tag{10}$$

$$\frac{\partial\Phi}{\partial t} = \frac{1}{Sc_1}\frac{\partial^2\Phi}{\partial y^2} - \gamma\Phi. \tag{11}$$

Dimensionless initial and boundary conditions becomes:

$$u(y,0)=0, \qquad \theta(y,0)=0, \qquad \Phi(y,0)=0,$$

$$u(0,t) = H(t)\cos(\omega t) \ or\ \sin(\omega t),$$

$$\theta(0,t) = \begin{cases} t, & 0<t\le 1 \\ 1, & t>1 \end{cases}, \tag{12}$$

$$\Phi(0,t) = \begin{cases} t, & 0<t\le 1 \\ 1, & t>1 \end{cases},$$

$$u(\infty,t)=0, \qquad \theta(\infty,t)=0, \qquad \Phi(\infty,t)=0,$$

During dimensionalization process we get some constants which are given below:

$$M^2 = \frac{\sigma_f a_0\beta_0^{\ 2}t_0}{\rho_f b_1}, \quad \Pr = \frac{(\mu C_p)_f}{k_f}, \quad Gr = \frac{g\beta_T(T_w-T_\infty)t_0}{U_0},$$

$$Gm = \frac{g\beta_C(C_w-C_\infty)t_0}{U_0}, \quad \frac{1}{K} = \frac{\mu_f t_0\phi}{k_1\rho_f}, \quad Nr = \frac{16\sigma_1 T_\infty^{\ 3}}{3k_3k_f},$$

$$P_0 = \frac{\Pr b_5}{\left(\lambda_{nf}+Nr\right)}, Sc = \frac{\upsilon}{D_f}, Sc_1 = \frac{Sc}{b_0}, \gamma = kt_0, H = M^2 + \frac{b_4}{B_0K},$$

$$b_0 = (1-\phi), b_1 = (1-\phi)+\phi\frac{\rho_s}{\rho_f}, b_2 = (1-\phi)+\phi\frac{(\rho\beta_T)_s}{(\rho\beta_T)_f},$$

$$b_3 = (1-\phi)+\phi\frac{(\rho\beta_C)_s}{(\rho\beta_C)_f}, \quad b_4 = \frac{1}{b_0^{\ 2.5}b_1}, \quad b_5 = (1-\phi)+\phi\frac{(\rho C_p)_s}{(\rho C_p)_f},$$

$$a_1 = \frac{1}{b_0^{\ 2.5}b_1B_0}, \qquad a_2 = \frac{b_2}{b_1}, \qquad a_3 = \frac{b_3}{b_1}.$$

3. EXACT SOLUTIONS

Applying the Laplace transforms to equations (9)-(11) and using the given initial conditions from equation (12), we get the following transform equations:

$$\frac{d^2\bar{u}}{dy^2}\mathrm{u}(y,s) - \left(\frac{s+H}{a_1}\right)\bar{u}(y,s) = -\frac{Gra_2\bar{\theta}(y,s)}{a_1} - \frac{Gma_3\bar{\Phi}(y,s)}{a_1}, \tag{13}$$

$$\frac{d^2\bar{\theta}}{dy^2} - sP_0\bar{\theta}(y,s) = 0, \tag{14}$$

$$\frac{d^2\bar{\Phi}}{dy^2} - Sc_1(s+\gamma)\bar{\Phi}(y,s) = 0. \tag{15}$$

After the Laplace Transform initial and boundary conditions from equation (12) are:

$$\bar{u}(y,0)=0, \qquad \bar{\theta}(y,0)=0, \qquad \bar{\Phi}(y,0)=0,$$

$$\bar{u}(0,s)=\frac{s}{s^2+\omega^2} \ or \ \frac{\omega}{s^2+\omega^2},$$

$$\bar{\theta}(0,s)=\begin{cases}\dfrac{1}{s^2}, & 0<t<1\\ \dfrac{1}{s}, & t>1\end{cases},$$

$$\bar{\Phi}(0,s)=\begin{cases}\dfrac{1}{s^2}, & 0<t<1\\ \dfrac{1}{s}, & t>1\end{cases}, \qquad (16)$$

$$\bar{u}(\infty,s)=0, \qquad \bar{\theta}(\infty,s)=0, \qquad \bar{\Phi}(\infty,s)=0.$$

Both ramped wall temperature and isothermal solutions of Eqs. (14) and (15) using corresponding boundary conditions from Eq.(16) are:

$$\bar{\theta}(y,s)_{ramp}=\frac{1}{s^2}e^{-y\sqrt{P_0 s}}, \qquad \bar{\theta}(y,s)_{iso}=\frac{1}{s}e^{-y\sqrt{P_0 s}}, \qquad (17)$$

$$\bar{\Phi}(y,s)_{ramp}=\frac{1}{s^2}e^{-y\sqrt{Sc_1(s+\gamma)}}, \bar{\Phi}(y,s)_{iso}=\frac{1}{s}e^{-y\sqrt{Sc_1(s+\gamma)}}. \qquad (18)$$

The inverse Laplace transforms of Eq. (17) is given below:

$$\theta(y,t)_{ramp}=\left[\left(t+\frac{y^2P_0}{2}\right)erfc\left(\frac{y}{2}\sqrt{\frac{P_0}{t}}\right)-y\sqrt{\frac{P_0 t}{\pi}}e^{-\frac{y^2P_0}{4t}}\right], \qquad (19)$$

$$\theta(y,t)_{iso}=erfc\left(\frac{y}{2}\sqrt{\frac{P_0}{t}}\right), \qquad (20)$$

where $\theta(y,t)_{ramp}$ and $\theta(y,t)_{iso}$ are the solutions of energy equation for the ramped and isothermal wall temperature respectively.

where the inverse Laplace transforms of Eq. (18) is given below:

$$\Phi(y,t)_{ramp}=\begin{bmatrix}e^{-y\sqrt{Sc_1\gamma}}erfc\left(\dfrac{y}{2}\sqrt{\dfrac{Sc_1}{t}}-\sqrt{\gamma t}\right)\left(\dfrac{t}{2}-\dfrac{y}{4}\sqrt{\dfrac{Sc_1}{\gamma}}\right)\\ +e^{y\sqrt{Sc_1\gamma}}erfc\left(\dfrac{y}{2}\sqrt{\dfrac{Sc_1}{t}}+\sqrt{\gamma t}\right)\left(\dfrac{t}{2}+\dfrac{y}{4}\sqrt{\dfrac{Sc_1}{\gamma}}\right)\end{bmatrix}, \qquad (21)$$

$$\Phi(y,t)_{iso}=\frac{1}{2}\begin{bmatrix}e^{-y\sqrt{Sc_1\gamma}}erfc\left(\dfrac{y}{2}\sqrt{\dfrac{Sc_1}{t}}-\sqrt{\gamma t}\right)\\ +e^{y\sqrt{Sc_1\gamma}}erfc\left(\dfrac{y}{2}\sqrt{\dfrac{Sc_1}{t}}+\sqrt{\gamma t}\right)\end{bmatrix}. \qquad (22)$$

where $\Phi(y,t)_{ramp}$ and $\Phi(y,t)_{iso}$ are the solutions of concentration equation for the ramped and isothermal wall temperature respectively.

The solution of Eq. (13) with the given initial and boundary conditions from Eq. (16) and incorporate equations (17) and (18) is given by:

$$\begin{aligned}\bar{u}_{c(ramp)}(y,s)&=\frac{s}{s^2+\omega^2}\exp\left(-y\sqrt{\frac{s+H}{a_1}}\right)\\ &+\frac{Gr_0}{s^2(s+H_1)}\exp\left(-y\sqrt{\frac{s+H}{a_1}}\right)\\ &+\frac{Gm_0}{s^2(s+H_2)}\exp\left(-y\sqrt{\frac{s+H}{a_1}}\right)\\ &-\frac{Gr_0}{s^2(s+H_1)}\exp\left(-y\sqrt{P_0 s}\right)\\ &-\frac{Gm_0}{s^2(s+H_2)}\exp\left(-y\sqrt{Sc_1(s+\gamma)}\right),\end{aligned} \qquad (23)$$

$$\begin{aligned}\bar{u}_{c(iso)}(y,s)&=\left[\frac{s}{s^2+\omega^2}+\frac{Gr_0}{s(s+H_1)}+\frac{Gm_0}{s(s+H_2)}\right]\exp\left(-y\sqrt{\frac{s+H}{a_1}}\right)\\ &-\frac{Gr_0}{s(s+H_1)}\exp\left(-y\sqrt{P_0 s}\right)\\ &-\frac{Gm_0}{s(s+H_2)}\exp\left(-y\sqrt{Sc_1(s+\gamma)}\right),\end{aligned} \qquad (24)$$

Applying partial fraction we get:

$$\begin{aligned}\bar{u}_{c(ramp)}(y,s)&=\left[\begin{matrix}\dfrac{1}{2(s+i\omega)}+\dfrac{1}{2(s-i\omega)}\\ -\dfrac{d_1}{s}+\dfrac{d_2}{s^2}+\dfrac{d_1}{(s+H_1)}\\ -\dfrac{d_3}{s}+\dfrac{d_4}{s^2}+\dfrac{d_3}{(s+H_2)}\end{matrix}\right]\exp\left(-y\sqrt{\frac{s+H}{a_1}}\right)\\ &+\left[\frac{d_1}{s}-\frac{d_2}{s^2}-\frac{d_1}{(s+H_1)}\right]\exp\left(-y\sqrt{P_0 s}\right),\\ &+\left[\frac{d_3}{s}-\frac{d_4}{s^2}-\frac{d_3}{(s+H_2)}\right]\exp\left(-y\sqrt{Sc_1(s+\gamma)}\right)\end{aligned} \qquad (25)$$

$$\begin{aligned}\bar{u}_{c(iso)}(y,s)&=\left[\begin{matrix}\dfrac{1}{2(s+i\omega)}+\dfrac{1}{2(s-i\omega)}\\ +\dfrac{d_2}{s}-\dfrac{d_2}{(s+H_1)}\\ +\dfrac{d_4}{s}-\dfrac{d_4}{(s+H_2)}\end{matrix}\right]\exp\left(-y\sqrt{\frac{s+H}{a_1}}\right)\\ &-\left[\frac{d_2}{s}-\frac{d_2}{(s+H_1)}\right]\exp\left(-y\sqrt{P_0 s}\right)\\ &-\left[\frac{d_4}{s}-\frac{d_4}{(s+H_2)}\right]\exp\left(-y\sqrt{Sc_1(s+\gamma)}\right)\end{aligned} \qquad (26)$$

3.1 Solutions for ramped wall temperature

Solution for cosine oscillation of the plate

$$\begin{aligned}\bar{u}_{c(ramp)}(y,s) &= \bar{u}_1(y,s)+\bar{u}_2(y,s)-d_5\bar{u}_3(y,s)\\ &+d_6\bar{u}_4(y,s)+d_1\bar{u}_5(y,s)+d_3\bar{u}_6(y,s)\\ &+d_1\bar{u}_7(y,s)-d_2\bar{u}_8(y,s)-d_1\bar{u}_9(y,s)\\ &+d_3\bar{u}_{10}(y,s)-d_4\bar{u}_{11}(y,s)-d_3\bar{u}_{12}(y,s).\end{aligned} \tag{27}$$

3.2 Solutions for isothermal plate

Solution for cosine oscillation of the plate

$$\begin{aligned}\bar{u}_{c(iso)}(y,s) &= \bar{u}_1(y,s)+\bar{u}_2(y,s)+d_6\bar{u}_3(y,s)\\ &-d_2\bar{u}_5(y,s)-d_4\bar{u}_6(y,s)-d_2\bar{u}_7(y,s)\\ &+d_2\bar{u}_9(y,s)-d_4\bar{u}_{10}(y,s)+d_4\bar{u}_{12}(y,s).\end{aligned} \tag{28}$$

$$Gr_0=\frac{Gra_2}{(P_0a_1-1)}, Gm_0=\frac{Gma_3}{(Sc_1a_1-1)}, H_1=\left(\frac{H}{1-P_0a_1}\right),$$

$$H_2=\left(\frac{Sc_1a_1\gamma-H}{Sc_1a_1-1}\right), d_1=\frac{Gr_0}{H_1^{\,2}}, d_2=\frac{Gr_0}{H_1}, d_3=\frac{Gm_0}{H_2^{\,2}},$$

$$d_4=\frac{Gm_0}{H_2}, \qquad d_5=d_1+d_3, \qquad d_6=d_2+d_4.$$

The inverse Laplace transforms of Eq. (27) is given by:

$$\begin{aligned}u_{c(ramp)}(y,t) &= u_1(y,t)+u_2(y,t)-d_5u_3(y,t)\\ &+d_6u_4(y,t)+d_1u_5(y,t)+d_3u_6(y,t)\\ &+d_1u_7(y,t)-d_2u_8(y,t)-d_1u_9(y,t)\\ &+d_3u_{10}(y,t)-d_4u_{11}(y,t)-d_3u_{12}(y,t)\end{aligned} \tag{29}$$

The inverse Laplace transform of Eq. (28) is given by:

$$\begin{aligned}u_{c(iso)}(y,t) &= u_1(y,t)+u_2(y,t)+d_6u_3(y,t)\\ &-d_2u_5(y,t)-d_4u_6(y,t)-d_2u_7(y,t)\\ &+d_2u_9(y,t)-d_4u_{10}(y,t)+d_4u_{12}(y,t).\end{aligned} \tag{30}$$

where $u_{c(ramp)}(y,t)$ and $u_{c(iso)}(y,t)$ are the velocity profiles for cosine oscillations for the ramped wall temperature and isothermal plate temperature respectively.
Where $u_i(y,s)$, $u_i(y,t)$, $i=1,2,3.....,12.$ are mentioned in the appendix.

4. LIMITING SOLUTIONS

4.1 Newtonian nanofluid, without Thermal radiation and chemical reaction

By putting radiation parameter $Nr=0$, chemical reaction parameter $\gamma=0$ and Casson fluid parameter $\beta\to\infty$ our solution reduced to the solution obtained by Kataria and Mittal [40]

Applying these limiting values we get new constant's which are given below:

$$P_0=\frac{\Pr b_5}{\lambda_{nf}}, \gamma=kt_0\to 0, H=M^2+\frac{b_4}{K}, a_1=\frac{1}{b_0^{\,2.5}b_1},$$

$$\bar{\theta}(y,s)_{ramp}=\frac{1}{s^2}e^{-y\sqrt{P_0s}}, \qquad \bar{\theta}(y,s)_{iso}=\frac{1}{s}e^{-y\sqrt{P_0s}}, \tag{31}$$

$$\bar{\Phi}(y,s)_{ramp}=\frac{1}{s^2}e^{-y\sqrt{Sc_1s}}, \qquad \bar{\Phi}(y,s)_{iso}=\frac{1}{s}e^{-y\sqrt{Sc_1s}}. \tag{32}$$

$$\begin{aligned}\bar{u}_{c(ramp)}(y,s) &= \frac{s}{s^2+\omega^2}\exp\left(-y\sqrt{\frac{s+H}{a_1}}\right)\\ &+\frac{Gr_0}{s^2(s+H_1)}\exp\left(-y\sqrt{\frac{s+H}{a_1}}\right)\\ &+\frac{Gm_0}{s^2(s+H_2)}\exp\left(-y\sqrt{\frac{s+H}{a_1}}\right)\\ &-\frac{Gr_0}{s^2(s+H_1)}\exp\left(-y\sqrt{P_0s}\right)\\ &-\frac{Gm_0}{s^2(s+H_2)}\exp\left(-y\sqrt{Sc_1s}\right),\end{aligned} \tag{33}$$

$$\begin{aligned}\bar{u}_{c(iso)}(y,s) &= \frac{s}{s^2+\omega^2}\exp\left(-y\sqrt{\frac{s+H}{a_1}}\right)\\ &+\frac{Gr_0}{s(s+H_1)}\exp\left(-y\sqrt{\frac{s+H}{a_1}}\right)\\ &+\frac{Gm_0}{s(s+H_2)}\exp\left(-y\sqrt{\frac{s+H}{a_1}}\right)\\ &-\frac{Gr_0}{s(s+H_1)}\exp\left(-y\sqrt{P_0s}\right)\\ &-\frac{Gm_0}{s(s+H_2)}\exp\left(-y\sqrt{Sc_1s}\right),\end{aligned} \tag{34}$$

$$\begin{aligned}\bar{u}_{c(ramp)}(y,s) &= \bar{u}_1(y,s)+\bar{u}_2(y,s)-d_5\bar{u}_3(y,s)\\ &+d_6\bar{u}_4(y,s)+d_1\bar{u}_5(y,s)+d_3\bar{u}_6(y,s)\\ &+d_1\bar{u}_7(y,s)-d_2\bar{u}_8(y,s)-d_1\bar{u}_9(y,s)\\ &+d_3\bar{u}_{10}(y,s)-d_4\bar{u}_{11}(y,s)-d_3\bar{u}_{12}(y,s).\end{aligned} \tag{35}$$

$$\begin{aligned}\bar{u}_{c(iso)}(y,s) &= \bar{u}_1(y,s)+\bar{u}_2(y,s)+d_6\bar{u}_3(y,s)\\ &-d_2\bar{u}_5(y,s)-d_4\bar{u}_6(y,s)-d_2\bar{u}_7(y,s)\\ &+d_2\bar{u}_9(y,s)-d_4\bar{u}_{10}(y,s)+d_4\bar{u}_{12}(y,s).\end{aligned} \tag{36}$$

$$\theta(y,t)_{ramp}=\left[\left(t+\frac{y^2P_0}{2}\right)erfc\left(\frac{y}{2}\sqrt{\frac{P_0}{t}}\right)-y\sqrt{\frac{P_0t}{\pi}}e^{-\frac{y^2P_0}{4t}}\right], \tag{37}$$

$$\theta(y,t)_{iso}=erfc\left(\frac{y}{2}\sqrt{\frac{P_0}{t}}\right), \tag{38}$$

$$\Phi(y,t)_{ramp}=\begin{bmatrix} e^{-y\sqrt{Sc_1\gamma}}erfc\left(\frac{y}{2}\sqrt{\frac{Sc_1}{t}}-\sqrt{\gamma t}\right)\left(\frac{t}{2}-\frac{y}{4}\sqrt{\frac{Sc_1}{\gamma}}\right) \\ +e^{y\sqrt{Sc_1\gamma}}erfc\left(\frac{y}{2}\sqrt{\frac{Sc_1}{t}}+\sqrt{\gamma t}\right)\left(\frac{t}{2}+\frac{y}{4}\sqrt{\frac{Sc_1}{\gamma}}\right)\end{bmatrix}, \quad (39)$$

$$\Phi(y,t)_{iso}=\frac{1}{2}\begin{bmatrix} e^{-y\sqrt{Sc_1\gamma}}erfc\left(\frac{y}{2}\sqrt{\frac{Sc_1}{t}}-\sqrt{\gamma t}\right) \\ +e^{y\sqrt{Sc_1\gamma}}erfc\left(\frac{y}{2}\sqrt{\frac{Sc_1}{t}}+\sqrt{\gamma t}\right)\end{bmatrix}. \quad (40)$$

$$\begin{aligned} u_{c(ramp)}(y,t)&=u_1(y,t)+u_2(y,t)-d_5u_3(y,t)\\ &+d_6u_4(y,t)+d_1u_5(y,t)+d_3u_6(y,t)\\ &+d_1u_7(y,t)-d_2u_8(y,t)-d_1u_9(y,t)\\ &+d_3u_{10}(y,t)-d_4u_{11}(y,t)-d_3u_{12}(y,t), \end{aligned} \quad (41)$$

$$\begin{aligned} u_{c(iso)}(y,t)&=u_1(y,t)+u_2(y,t)+d_6u_3(y,t)\\ &-d_2u_5(y,t)-d_4u_6(y,t)-d_2u_7(y,t)\\ &+d_2u_9(y,t)-d_4u_{10}(y,t)+d_4u_{12}(y,t), \end{aligned} \quad (42)$$

4.2 Newtonian nanofluid without thermal radiation and Mass transfer

By putting radiation parameter $Nr=0$, $\beta\to\infty$ and $Gm=0$ then our solutions reduces to the solutions obtained by Khalid et al. [37]

In the absence of concentration profile our solutions are quite identical to.[37] and the constants produces in the following form:

$$Gm=0, P_0=\frac{\Pr b_5}{\lambda_{nf}}, H=M^2+\frac{b_4}{K}, a_1=\frac{1}{b_0^{2.5}b_1}, d_3=0, d_4=0,$$

$$\bar{\theta}(y,s)_{ramp}=\frac{1}{s^2}e^{-y\sqrt{P_0 s}}, \qquad \bar{\theta}(y,s)_{iso}=\frac{1}{s}e^{-y\sqrt{P_0 s}}, \quad (43)$$

$$\begin{aligned} \bar{u}_{c(ramp)}(y,s)&=\left[\frac{s}{s^2+\omega^2}+\frac{Gr_0}{s^2(s+H_1)}\right]\exp\left(-y\sqrt{\frac{s+H}{a_1}}\right)\\ &-\frac{Gr_0}{s^2(s+H_1)}\exp\left(-y\sqrt{P_0 s}\right) \end{aligned} \quad (44)$$

$$\begin{aligned} \bar{u}_{c(iso)}(y,s)&=\left[\frac{s}{s^2+\omega^2}+\frac{Gr_0}{s(s+H_1)}\right]\exp\left(-y\sqrt{\frac{s+H}{a_1}}\right)\\ &-\frac{Gr_0}{s(s+H_1)}\exp\left(-y\sqrt{P_0 s}\right) \end{aligned} \quad (45)$$

$$\begin{aligned} \bar{u}_{c(ramp)}(y,s)&=\bar{u}_1(y,s)+\bar{u}_2(y,s)-d_5\bar{u}_3(y,s)\\ &+d_6\bar{u}_4(y,s)+d_1\bar{u}_5(y,s)+d_1\bar{u}_7(y,s)\\ &-d_2\bar{u}_8(y,s)-d_1\bar{u}_9(y,s) \end{aligned} \quad (46)$$

$$\begin{aligned} \bar{u}_{c(iso)}(y,s)&=\bar{u}_1(y,s)+\bar{u}_2(y,s)+d_6\bar{u}_3(y,s)\\ &-d_2\bar{u}_5(y,s)-d_2\bar{u}_7(y,s)+d_2\bar{u}_9(y,s). \end{aligned} \quad (47)$$

$$\theta(y,t)_{ramp}=\left[\left(t+\frac{y^2P_0}{2}\right)erfc\left(\frac{y}{2}\sqrt{\frac{P_0}{t}}\right)-y\sqrt{\frac{P_0 t}{\pi}}e^{-\frac{y^2P_0}{4t}}\right], \quad (48)$$

$$\theta(y,t)_{iso}=erfc\left(\frac{y}{2}\sqrt{\frac{P_0}{t}}\right), \quad (49)$$

$$\begin{aligned} u_{c(ramp)}(y,t)&=u_1(y,t)+u_2(y,t)-d_5u_3(y,t)\\ &+d_6u_4(y,t)+d_1u_5(y,t)+d_1u_7(y,t)\\ &-d_2u_8(y,t)-d_1u_9(y,t). \end{aligned} \quad (50)$$

$$\begin{aligned} u_{c(iso)}(y,t)&=u_1(y,t)+u_2(y,t)+d_6u_3(y,t)\\ &-d_2u_5(y,t)-d_2u_7(y,t)+d_2u_9(y,t). \end{aligned} \quad (51)$$

5. NUSSELT NUMBER, SHERWOOD NUMBER AND SKIN FEICTION

5.1 Nusselt number

The Nusselt number Nu s written as:

$$Nu=-k_{nf}\left(\frac{\partial\theta(y,t)}{\partial y}\right)_{y=0} \quad (52)$$

5.2 Sherwood number

The Sherwood number S_h is written as

$$S_h=-D_{nf}\left(\frac{\partial\Phi(y,t)}{\partial y}\right)_{y=0}. \quad (53)$$

5.3 Skin friction

The Skin Friction τ is written as

$$\tau=-\frac{1}{(1-\phi)^{2.5}}\left(1+\frac{1}{\beta}\right)\left(\frac{\partial u(y,t)}{\partial y}\right)_{y=0}. \quad (54)$$

6. RESULTS AND DISCUSSION

In this section, to understand the physics of the problem, the obtained exact solutions are studied numerically and discussed the effect of all embedded parameters by graphical analysis. During the parametric study the effect of volume friction parameter ϕ , permeability of porous medium K , magnetic parameter M , Grashop number Gr , mass Grashop number Gm , Schmidth number Sc and Casson parameter β , chemical reaction parameter γ and phase angle ωt are described graphically in Figs. 2-10 for velocity profile. The effect of radiation parameter Nr Fig.11 for temperature profile. The effect of chemical reaction parameter γ and Schmidth number Sc are described in Figs. 12, 13 for concentration profile. Numerical values for skin-friction, Nusselt number and Sherwood number are computed and presented in tables for different parameters.

Geometry of the problem is shown in Figs. 1. Fig. 2 shows the effect of volume fraction parameter ϕ of nanoparticles on the nanofluid velocity. By increasing volume fraction parameter the nanofluid velocity decreases for both cases of ramped wall temperature and isothermal boundary condition. Because increasing the volume fraction parameter the velocity of the fluid decreasing because when the volume fraction is increases then their exists maximum number of friction forces due to this fact velocity decreases. The results are plotted for volume fraction parameter for cosine oscillations as shown in figure. Fig. 3 depicts the effect of permeability parameter K on velocity profile by keeping other parameter fixed. Nanofluid velocity increases by increasing permeability parameter because it decreases resistance of the fluid. Fig. 4 illustrates that nanofluid velocity decreases with the increase in magnetic parameter M. By increasing magnetic parameter, it produces turbulency in the fluid as a result there exist maximum number of friction forces and behavior of the fluid become more viscous due to which nanofluid velocity decreases. Fig.5 exhibits velocity profiles for different values of Grashof number Gr and keeping other values constant. Inceasing Gr results an increase in the buoyancy forces which increase the nanofluid velocity. Grashop number of the velocity is known as buoyancy forces by increasing these boyancy forces the viscosity of the fluid decreases as a result the fluid velocity increases with the increase of these forces which is called Gr. Fig.6 shows the effect of mass Grashop number Gm on the fluid velocity. Velocity of the fluid increases by increasing Gm. Fig.7 displays the effect of Schmidth number Sc on the nanofluid velocity. It has been observed that by increasing Sc deccreases the nanofluid velocity. Fig. 8 shows the effect of Casson fluid parameter β on the nanofluid velocity. From this figure, it is observed that Casson fluid parameter decreases the nanofluid velocity. Fig.9 depicts the effect of chemical reaction parameter γ on velocity profile. From this figure it has been observed that by increasing chemical reaction parameter γ velocity of the nanofluid decreases. Chemical reaction change the behavior of the fluid and make the fluid more denser therefore the velocity of the denser fluid is minimum.Fig.10 shows the effect of phase angle on the nanofluid velocity keeping other values fixed. Fig.11 depicts that temperature profile increases by increasing radiation parameter Nr by keeping other values constant. The temperature of the fluid increases with increase in radiation parameter. This behavior shows that rate of radiation emitted from the fluid is directly proportional to temperature. It is depicted from Fig.12 that by increasing the value of chemical reaction parameter γ there is a decrease in concentration of the fluid. The species of the fluid is increases there is a decrease in the concentration profile due to the reaction in the fluid. Fig. 13 shows the effect of Schmidth number on concentration profile. When we increase the values of Schmidth number the concentration of the fluid is decreased. Figure 2-10 explained velocity profile for different parameters. All the figures illustrate cosine oscillation for the velocity profile. And the behaviors of all parameters are explained for ramped wall and isothermal conditions and compare their results graphically.

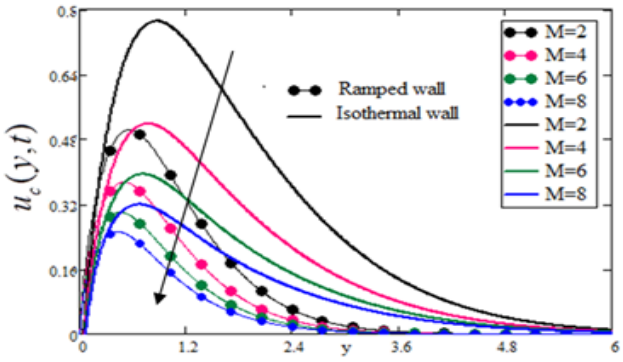

Figure 4. Velocity profiles for magnetic parameter M keeping other parameter constant

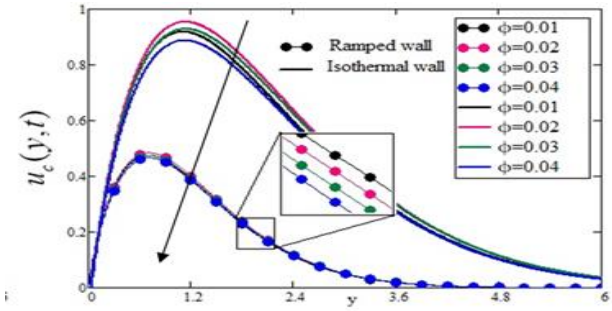

Figure 2. The velocity profiles for different values of volume friction ϕ keeping othervalues constant

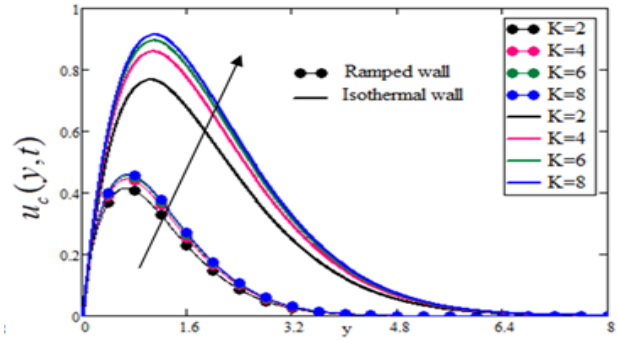

Figure 3. Velocity profiles for different values of porosity parameter K

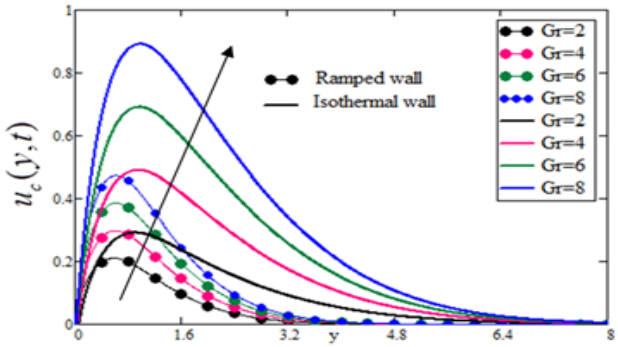

Figure 5. Velocity profiles for different values of Grashop number Gr keeping other parameters fixed

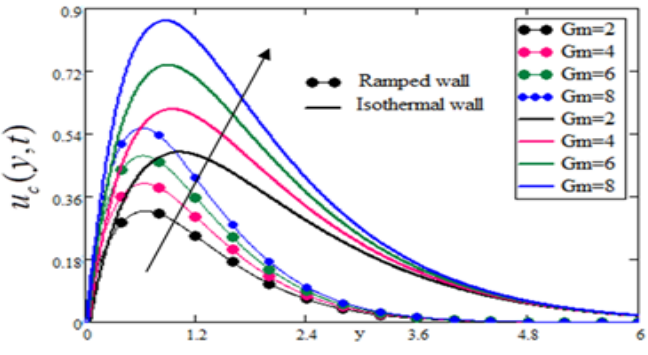

Figure 6. Velocity profiles for different values of mass Grashof number *Gm*

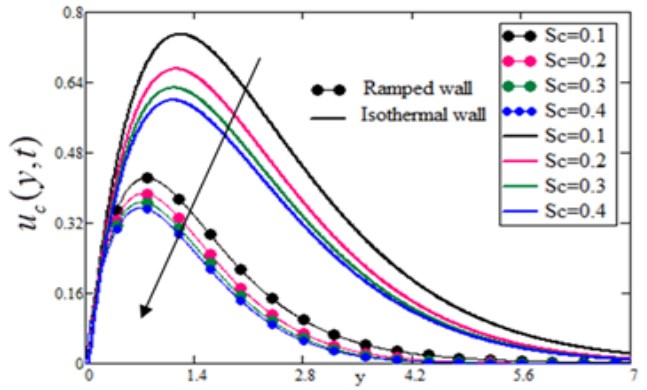

Figure 7. Velocity profiles for different values of *Sc* keeping other parameters fixed

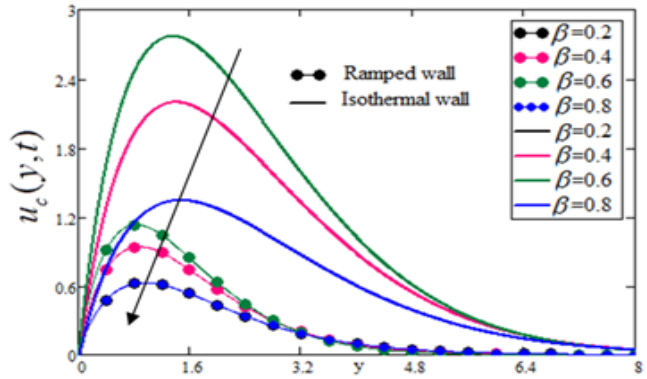

Figure 8. Velocity profiles for different values of Casson fluid parameter β

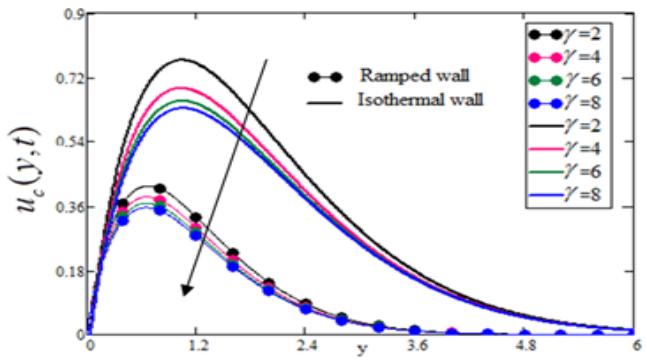

Figure 9. Velocity profiles for different values of chemical reaction parameter γ taking other values constant

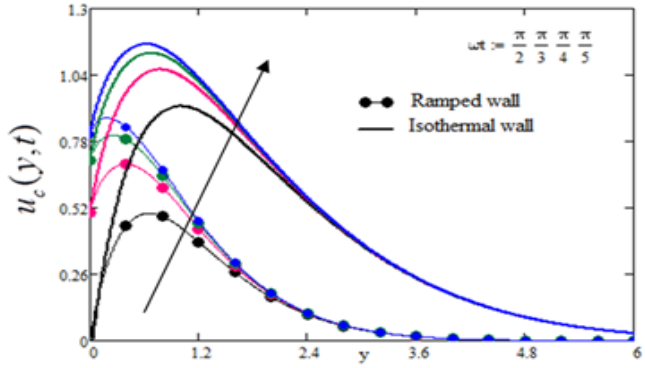

Figure 10. Velocity profiles for different values of phase angle ωt keeping other values constant

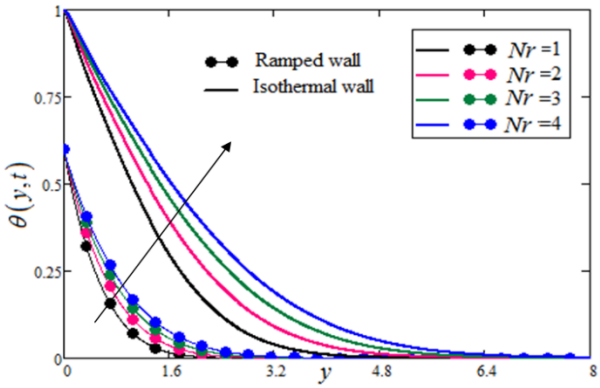

Figure 11. Temperature profiles for different Values of radiation parameter Nr keeping other values constant

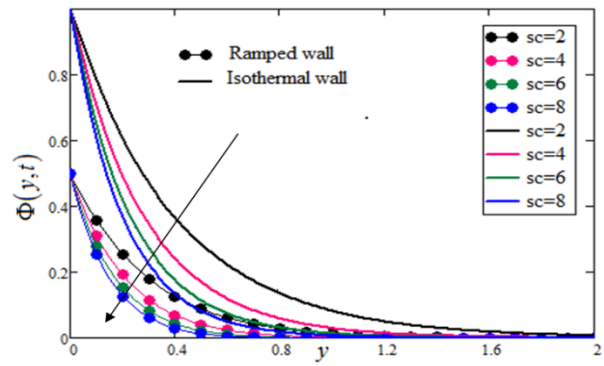

Figure 12. Concentration profiles for different values of Schmidth number Sc keeping other values fixed

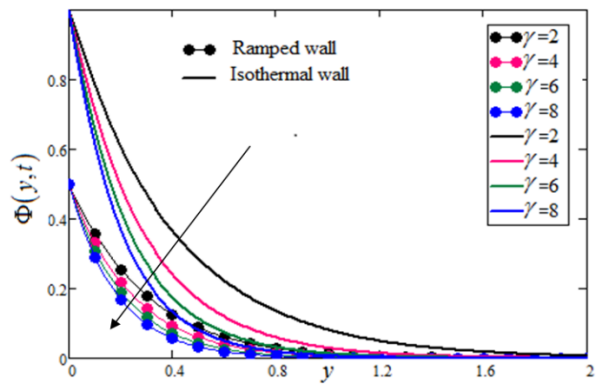

Figure 13. Concentration profiles for different values of chemical reaction γ keeping other values fixed

Table 2. Skin friction variation for isothermal and ramped wall temperature

Nr	β	Gr	Gm	Sc	M	ωt	ϕ	t	k	t_0	C_{fiso}	C_{fram}
2.5	2.5	2	2	0.5	2	$\frac{\pi}{4}$	0.02	0.9	2	1.9	0.302	3.405
3	2.5	2	2	0.5	2	$\frac{\pi}{4}$	0.02	0.9	2	1.9	0.317	3.439
2.5	**3**	2	2	0.5	2	$\frac{\pi}{4}$	0.02	0.9	2	1.9	0.318	3.36
2.5	2.5	**3**	2	0.5	2	$\frac{\pi}{4}$	0.02	0.9	2	1.9	0.624	4.245
2.5	2.5	2	**3**	0.5	2	$\frac{\pi}{4}$	0.02	0.9	2	1.9	0.433	3.712
2.5	2.5	2	2	**1**	2	$\frac{\pi}{4}$	0.02	0.9	2	1.9	0.187	3.318
2.5	2.5	2	2	0.5	**3**	$\frac{\pi}{4}$	0.02	0.9	2	1.9	0.095	3.194
2.5	2.5	2	2	0.5	2	$\frac{\boldsymbol{\pi}}{\mathbf{3}}$	0.02	0.9	2	1.9	0.75	4.424
2.5	2.5	2	2	0.5	2	$\frac{\pi}{4}$	**0.03**	0.9	2	1.9	0.242	3.337
2.5	2.5	2	2	0.5	2	$\frac{\pi}{4}$	0.02	**0.8**	2	1.9	-	0.024
2.5	2.5	2	2	0.5	2	$\frac{\pi}{4}$	0.02	0.9	**3**	1.9	0.275	3.345
2.5	2.5	2	2	0.5	2	$\frac{\pi}{4}$	0.02	0.9	2	**1.8**	3.027	-

Table 3. Nusselt number variation for isothermal and ramped wall temperature

t	t_0	Nr	ϕ	Nu_{iso}	Nu_{ram}
0.6	1.6	1	0.02	-0.228	-0.372
0.7	1.6	1	0.02	-0.228	-0.345
0.6	**1.7**	1	0.02	-0.215	-0.372
0.6	1.6	**2**	0.02	-0.186	-0.304
0.6	1.6	1	**0.04**	-0.234	-0.381

Table 4. Sherwood number variation for isothermal and ramped wall temperature

t	t_0	Sc	K	ϕ	S_{hiso}	S_{hram}
0.6	1.6	5	2	0.02	-4.906	-4.295
0.7	1.6	5	2	0.02	-4.906	-4.4
0.6	**1.8**	5	2	0.02	-5.328	-4.641
0.6	1.6	**6**	2	0.02	-5.374	-4.705
0.6	1.6	5	**3**	0.02	-6.246	-5.593
0.6	1.6	5	2	**0.04**	-5.219	-4.569

7. CONCLUDING REMARKS

An exact solution is obtained for the unsteady MHD Casson nanofluid bounded by an infinite oscillating vertical plate. Nanofluid is formed by suspending MoS_2 nanoparticles in Polyethylene glycol (PEG) liquid. The problems is solved for exact solution and the expressions for velocity, temperature and concentration are obtained using Laplace transform technique. The obtained solutions satisfy the initial and boundary conditions and the governing partial differential equations can be reduced to the well-known published results, which shows the validity of the present work. Both cases of ramped wall temperature and isothermal boundary conditions of the plate are discussed. From graphical analysis, it is observed that the velocity, temperature and concentration profiles are greater for isothermal temperature as compared to ramped wall temperature. The numerical values are evaluated for skin friction, Nusselt number and Sherwood number and presented in tabular forms. The following main results are concluded during the solutions of the problem and graphical analysis.

- The effect of volume fraction parameter ϕ are shown in velocity profile. By increasing ϕ the temperature of the fluid is increasing because the fluid particles volume is increases. These particles collide with each other and there produce kinetic energy (K.E) in the fluid and by increasing kinetic energy (K.E) the temperature of the fluid is increases due to this reason the fluid velocity decreases.
- From the whole graphical results we noticed that the magnitude of velocity, temperature and concentration profiles are smaller for ramped wall temperature and greater for isothermal temperature.
- Increasing porosity K velocity of nanofluid increases. When the porosity of the medium is increases the friction forces decreases due to which velocity of the fluid is increases.
- Velocity of the fluid increases by increasing the values of Sc.
- The effect of radiation parameter Nr , is directly proportional to the temperature by increasing Nr the temperature of the fluid is increases
- Chemical reaction parameter γ and Schmidt number Sc decreases the concentration by decreasing their values.
- Increase in the volume fraction of nanoparticles, increases the heat transfer rate.

REFERENCES

[1] Di Matteo P, Donsi G, Ferrari G. (2003). The role of heat and mass transfer phenomena in atmospheric freeze-drying of foods in a fluidised bed. Journal of Food Engineering 59(2): 267-275. https://doi.org/10.18280/10.1016/S0260-

8774(02)00467-3
[2] Blums E. (2002). Heat and mass transfer phenomena. In Ferrofluids. Springer, Berlin, Heidelberg, pp. 124-139.
[3] Bergman TL, Incropera FP, DeWitt DP, Lavine AS. (2011). Fundamentals of heat and mass transfer. John Wiley & Sons.
[4] Nield DA, Bejan A, Bejan N. (2006). Convection in porous media. New York: Springer 3.
[5] Choi SUS. (1995). Enhancing thermal conductivity of fluids with nanoparticles. ASME-Publications-Fed 231: 99-106. ANL/MSD/CP-84938; CONF-951135-29.
[6] Choi SUS, Zhang ZG, Yu W, Lockwood FE, Grulke EA. (2001). Anomalous thermal conductivity enhancement in nanotube suspensions. Applied Physicsletters 79(14): 2252-2254. https://doi.org/10.18280/10.1063/1.1408272
[7] Li S, Eastman JA. (1999). Measuring thermal conductivity of fluids containing oxide nanoparticles. J. Heat Transf. 121(2): 280-289. https://doi.org/10.18280/10.1115/1.2825978
[8] Masuda H, Ebata A, Teramae K. (1993). Alteration of thermal conductivity and viscosity of liquid by dispersing ultra-fine particles. Dispersion of Al_2O_3, SiO_2 and TiO_2 Ultra-fine Particles 7(4). https://doi.org/10.18280/10.2963/jjtp.7.227
[9] Xuan Y, Roetzel W. (2000). Conceptions for heat transfer correlation of nanofluids. International Journal of Heat and Mass Transfer 43(19): 3701-3707. https://doi.org/10.18280/10.1016/S0017-9310(99)00369-5
[10] Wakif A, Boulahia Z, Sehaqui R. (2017). Numerical analysis of the onset of longitudinal convective rolls in a porous medium saturated by an electrically conducting nanofluid in the presence of an external magnetic field. Results in Physics. 7: 2134-2152. https://doi.org/10.18280/10.1016/j.rinp.2017.06.003
[11] Ali F, Aamina B, Khan I, Sheikh NA, Saqib M. (2017). Magnetohydrodynamic flow of brinkman-type engine oil based MoS_2-nanofluid in a rotating disk with hall effect. Int J Heat Technol 35(4): 893-902. https://doi.org/10.18280/1018280/ijht.350426
[12] Casson, N. (1959). A flow equation for pigment-oil suspensions of the printing ink type. Rheology of disperse systems. Pergamon Press.
[13] Dash RK, Mehta KN, Jayaraman G. (1996). Casson fluid flow in a pipe filled with a homogeneous porous medium. International Journal of Engineering Science 34(10): 1145-1156. https://doi.org/10.18280/10.1016/0020-7225(96)00012-2
[14] Akbar NS. (2015). Influence of magnetic field on peristaltic flow of a Casson fluid in an asymmetric channel: application in crude oil refinement. Journal of Magnetism and Magnetic Materials 378: 463-468. https://doi.org/10.1016/j.jmmm.2014.11.045
[15] Noreen SA, Butt AW. (2015). Physiological transportation of Casson fluid in a plumb duct. Communications in Theoretical Physics 63(3): 347. https://doi.org/10.18280/10.1088/0253-6102/63/3/347
[16] Nadeem S, Haq RU, Akbar NS, Khan ZH. (2013). MHD three- dimensional Casson fluid flow past a porous linearly stretching sheet. Alexandria Engineering Journal 52(4): 577-582. https://doi.org/10.18280/10.1016/j.aej.2013.08.005
[17] Nadeem S, Haq RU, Akbar NS. (2014). MHD three-dimensional boundary layer flow of Casson nanofluid past a linearly stretching sheet with convective boundary condition. IEEE Transactions on Nanotechnology 13(1): 109-115. https://doi.org/10.18280/10.1109/TNANO.2013.2293735
[18] Saqib M, Ali F, Khan I, Sheikh NA. (2016). Heat and mass transfer phenomena in the flow of Casson fluid over an infinite oscillating plate in the presence of first-order chemical reaction and slip effect. Neural Computing and Applications 1-14. https://doi.org/10.18280/10.1007/s00521-016-2810-x
[19] Raju CSK, Sandeep N, Saleem S. (2016). Effects of induced magnetic field and homogeneous–heterogeneous reactions on stagnation flow of a Casson fluid. Engineering Science and Technology, an International Journal 19(2): 875-887. https://doi.org/10.18280/10.1016/j.jestch.2015.12.004
[20] Qing J, Bhatti MM, Abbas MA, Rashidi MM, Ali MES. (2016). Entropy generation on MHD Casson nanofluid flow over a porous stretching/shrinking surface. Entropy 18(4): 123. https://doi.org/10.18280/10.3390/e18040123
[21] Mustafa M, Khan JA. (2015). Model for flow of Casson nanofluid past a non linearly stretching sheet considering magnetic field effects. AIP Advances 5(7): 077148. https://doi.org/10.18280/10.1063/1.4927449
[22] Haq R, Nadeem S, Khan Z, Okedayo T. (2014). Convective heat transfer and MHD effects on Casson nanofluid flow over a shrinking sheet. Open Physics 12(12): 862-871. https://doi.org/10.18280/10.2478/s11534-014-0522-3
[23] Nadeem S, Mehmood R, Akbar NS. (2014). Optimized analytical solution for oblique flow of a Casson nanofluid with convective boundary conditions. International Journal of Thermal Sciences 78: 90-100. https://doi.org/10.18280/10.1016/j.ijthermalsci.2013.12.001
[24] Hussain T, Shehzad SA, Alsaedi A, Hayat T, Ramzan M. (2015). Flow of Casson nanofluid with viscous dissipation and convective conditions: a mathematical model. Journal of Central South University 22(3): 1132-1140. https://doi.org/10.18280/10.1007/s11771-015-2625-4
[25] Kim YJ. (2000). Unsteady MHD convective heat transfer past a semi-infinite vertical porous moving plate with variable suction. International Journal of Engineering Science 38(8): 833-845. https://doi.org/10.18280/10.1016/S0020-7225(99)00063-4
[26] Meier DL, Koide S, Uchida Y. (2001). Magnetohydrodynamic production of relativistic jets. Science 291(5501): 84-92. https://doi.org/10.18280/10.1126/science.291.5501.84
[27] Kataria HR, Patel HR. (2016). Radiation and chemical reaction effects on MHD Casson fluid flow past an oscillating vertical plate embedded in porous medium. Alexandria Engineering Journal 55(1): 583-595. https://doi.org/10.18280/10.1016/j.aej.2016.01.019
[28] Ali F, Gohar M, Khan I. (2016). MHD flow of water-based Brinkman type nanofluid over a vertical plate embedded in a porous medium with variable surface velocity, temperature and concentration. Journal of Molecular Liquids 223: 412-419. https://doi.org/10.18280/10.1016/j.molliq.2016.08.068

[29] Tadmor Z, Gogos CG. (2013). Principles of polymer processing. John Wiley & Sons, New Jersey. pp. 748-6011.
[30] Cussler EL. (2009). Diffusion: mass transfer in fluid systems. Cambridge University Press, New York, pp. 1-631.
[31] Salem AM, El-Aziz MA. (2008). Effect of Hall currents and chemical reaction on hydromagnetic flow of a stretching vertical surface with internal heat generation/absorption. Applied Mathematical Modelling 32(7): 1236-1254. https://doi.org/10.18280/10.1016/j.apm.2007.03.008
[32] Rajesh V. (2010). Radiation and chemical reaction effects on flow past a vertical plate with ramped wall temperature. Ann J Eng. 8(Fascicule 3): 426-433.
[33] Kelleher M. (1971). Free convection from a vertical plate with discontinuous wall temperature. ASME J. Heat Transfer 93(4): 349-356. https://doi.org/10.18280/10.1115/1.3449830
[34] Kao TT. (1975). Laminar free convective heat transfer response along a vertical flat plate with step jump in surface temperature. Letters in Heat and Mass Transfer 2(5): 419-428. https://doi.org/10.18280/10.1016/0094-4548(75)90008-9
[35] Chandran P, Sacheti NC, Singh AK. (2005). Natural convection near a vertical plate with ramped wall temperature. Heat and Mass Transfer 41(5): 459-464. https://doi.org/10.18280/10.1007/s00231-004-0568-7
[36] Seth GS, Ansari MS, Nandkeolyar R. (2011). MHD natural convection flow with radiative heat transfer past an impulsively moving plate with ramped wall temperature. Heat and Mass Transfer 47(5): 551-561. https://doi.org/10.18280/10.1007/s00231-010-0740-1
[37] Narahari M, Bég OA. (2010). Radiation effects on free convection flow past an impulsively started infinite vertical plate with ramped wall temperature and constant mass diffusion. In M. A. Wahid, S. Samion, N. A. C. Sidik, & J. M. Sheriff (Eds.), AIP Conference Proceedings 1225(1): 743-750.
[38] Khalid A, Khan I, Shafie S. (2015). Exact solutions for free convection flow of nanofluids with ramped wall temperature. The European Physical Journal Plus 130(4): 57. https://doi.org/10.18280/10.1140/epjp/i2015-15057-9
[39] Khan I, Ali F, Shafie S. (2012). MHD free convection flow in a porous medium with thermal diffusion and ramped wall temperature. Journal of the Physical Society of Japan 81(4): 044401. https://doi.org/10.18280/10.1143/JPSJ.81.044401
[40] Nandkeolyar R, Das M, Pattnayak H. (2013). Unsteady hydromagnetic radiative flow of a nanofluid past a flat plate with ramped temperature. Journal of the Orissa Mathematical Society 975: 2323.
[41] Kataria HR, Mittal AS. (2017). Velocity, mass and temperature analysis of gravity-driven convection nanofluid flow past an oscillating vertical plate in the presence of magnetic field in a porous medium. Applied Thermal Engineering 110: 864-874. https://doi.org/10.18280/10.1016/j.applthermaleng.2016.08.129
[42] Kakac S, Pramuanjaroenkij A. (2009). Review of convective heat transfer enhancement with nanofluids, Int. J. Heat Mass Transfer 52: 3187–3196. https://doi.org/10.18280/10.1016/j.ijheatmasstransfer.2009.02.006
[43] Oztop HF, Abu-Nada E. (2008). Numerical study of natural convection in partially heated rectangular enclosures filled with nanofluids. International Journal of Heat and Fluid Flow 29(5): 1326-1336. https://doi.org/10.18280/10.1016/j.ijheatfluidflow.2008.04.009

APPENDIX

$$\bar{u}_1(y,s)=\frac{1}{2(s+i\omega)}\exp\left(-y\sqrt{\frac{s+H}{a_1}}\right),$$

$$\bar{u}_2(y,s)=\frac{1}{2(s-i\omega)}\exp\left(-y\sqrt{\frac{s+H}{a_1}}\right),$$

$$\bar{u}_3(y,s)=\frac{1}{s}\exp\left(-y\sqrt{\frac{s+H}{a_1}}\right),$$

$$\bar{u}_4(y,s)=\frac{1}{s^2}\exp\left(-y\sqrt{\frac{s+H}{a_1}}\right),$$

$$\bar{u}_5(y,s)=\frac{1}{(s+H_1)}\exp\left(-y\sqrt{\frac{s+H}{a_1}}\right),$$

$$\bar{u}_6(y,s)=\frac{1}{(s+H_2)}\exp\left(-y\sqrt{\frac{s+H}{a_1}}\right),$$

$$\bar{u}_7(y,s)=\frac{1}{s}\exp\left(-y\sqrt{P_0 s}\right),$$

$$\bar{u}_8(y,s)=\frac{1}{s^2}\exp\left(-y\sqrt{P_0 s}\right),$$

$$\bar{u}_9(y,s)=\frac{1}{(s+H_1)}\exp\left(-y\sqrt{P_0 s}\right),$$

$$\bar{u}_{10}(y,s)=\frac{1}{s}\exp\left(-y\sqrt{Sc_1(s+\gamma)}\right),$$

$$\bar{u}_{11}(y,s)=\frac{1}{s^2}\exp\left(-y\sqrt{Sc_1(s+\gamma)}\right),$$

$$\bar{u}_{12}(y,s)=\frac{1}{(s+H_2)}\exp\left(-y\sqrt{Sc_1(s+\gamma)}\right),$$

$$u_1(y,t)=\frac{e^{-i\omega t}}{4}\left[\begin{array}{l}e^{-y\sqrt{\frac{H+i\omega}{a_1}}}\,erfc\left(\frac{y}{2\sqrt{a_1 t}}-\sqrt{(H+i\omega)t}\right)\\+e^{y\sqrt{\frac{H+i\omega}{a_1}}}\,erfc\left(\frac{y}{2\sqrt{a_1 t}}+\sqrt{(H+i\omega)t}\right)\end{array}\right],$$

$$u_2(y,t)=\frac{e^{i\omega t}}{4}\left[\begin{array}{l}e^{-y\sqrt{\frac{H-i\omega}{a_1}}}\,erfc\left(\frac{y}{2\sqrt{a_1 t}}-\sqrt{(H-i\omega)t}\right)\\+e^{y\sqrt{\frac{H-i\omega}{a_1}}}\,erfc\left(\frac{y}{2\sqrt{a_1 t}}+\sqrt{(H-i\omega)t}\right)\end{array}\right],$$

$$u_3(y,t)=\frac{1}{2}\left[\begin{array}{l}e^{-y\sqrt{\frac{H}{a_1}}}\,erfc\left(\frac{y}{2\sqrt{a_1 t}}-\sqrt{Ht}\right)\\+e^{y\sqrt{\frac{H}{a_1}}}\,erfc\left(\frac{y}{2\sqrt{a_1 t}}+\sqrt{Ht}\right)\end{array}\right],$$

$$u_4(y,t)=\begin{bmatrix} e^{-y\sqrt{\frac{H}{a_1}}}erfc\left(\frac{y}{2\sqrt{a_1t}}-\sqrt{Ht}\right)\left(\frac{t}{2}-\frac{y}{4\sqrt{a_1H}}\right) \\ +e^{y\sqrt{\frac{H}{a_1}}}erfc\left(\frac{y}{2\sqrt{a_1t}}+\sqrt{Ht}\right)\left(\frac{t}{2}+\frac{y}{4\sqrt{a_1H}}\right)\end{bmatrix},$$

$$u_5(y,t)=\frac{e^{-H_1t}}{2}\begin{bmatrix} e^{-y\sqrt{\frac{H_1+H}{a_1}}}erfc\left(\frac{y}{2\sqrt{a_1t}}-\sqrt{(H_1+H)t}\right) \\ +e^{y\sqrt{\frac{H_1+H}{a_1}}}erfc\left(\frac{y}{2\sqrt{a_1t}}+\sqrt{(H_1+H)t}\right)\end{bmatrix},$$

$$u_6(y,t)=\frac{e^{-H_2t}}{2}\begin{bmatrix} e^{-y\sqrt{\frac{H_2+H}{a_1}}}erfc\left(\frac{y}{2\sqrt{a_1t}}-\sqrt{(H_2+H)t}\right) \\ +e^{y\sqrt{\frac{H_2+H}{a_1}}}erfc\left(\frac{y}{2\sqrt{a_1t}}+\sqrt{(H_2+H)t}\right)\end{bmatrix},$$

$$u_7(y,t)=erfc\left(\frac{y}{2}\sqrt{\frac{P_0}{t}}\right),$$

$$u_8(y,t)=\left[\left(t+\frac{y^2P_0}{2}\right)erfc\left(\frac{y}{2}\sqrt{\frac{P_0}{t}}\right)-y\sqrt{\frac{P_0t}{\pi}}e^{\frac{-y^2P_0}{4t}}\right],$$

$$u_9(y,t)=\frac{e^{-H_1t}}{2}\begin{bmatrix} e^{-y\sqrt{P_0H_1}}erfc\left(\frac{y}{2}\sqrt{\frac{P_0}{t}}-\sqrt{H_1t}\right) \\ +e^{y\sqrt{P_0H_1}}erfc\left(\frac{y}{2}\sqrt{\frac{P_0}{t}}+\sqrt{H_1t}\right)\end{bmatrix},$$

$$u_{10}(y,t)=\frac{1}{2}\begin{bmatrix} e^{-y\sqrt{Sc_1\gamma}}erfc\left(\frac{y}{2}\sqrt{\frac{Sc_1}{t}}-\sqrt{\gamma t}\right) \\ +e^{y\sqrt{Sc_1\gamma}}erfc\left(\frac{y}{2}\sqrt{\frac{Sc_1}{t}}+\sqrt{\gamma t}\right)\end{bmatrix},$$

$$u_{11}(y,t)=\begin{bmatrix} e^{-y\sqrt{Sc_1\gamma}}erfc\left(\frac{y}{2}\sqrt{\frac{Sc_1}{t}}-\sqrt{\gamma t}\right)\left(\frac{t}{2}-\frac{y}{4}\sqrt{\frac{Sc_1}{\gamma}}\right) \\ +e^{y\sqrt{Sc_1\gamma}}erfc\left(\frac{y}{2}\sqrt{\frac{Sc_1}{t}}+\sqrt{\gamma t}\right)\left(\frac{t}{2}+\frac{y}{4}\sqrt{\frac{Sc_1}{\gamma}}\right)\end{bmatrix},$$

$$u_{12}(y,t)=\frac{e^{-H_2t}}{2}\begin{bmatrix} e^{-y\sqrt{Sc_1}\sqrt{H_2+\gamma}}erfc\left(\frac{y}{2}\sqrt{\frac{Sc_1}{t}}-\sqrt{(H_2+\gamma)t}\right) \\ +e^{y\sqrt{Sc_1}\sqrt{H_2+\gamma}}erfc\left(\frac{y}{2}\sqrt{\frac{Sc_1}{t}}+\sqrt{(H_2+\gamma)t}\right)\end{bmatrix}.$$